PAPER • OPEN ACCESS

Structure of surface electronic states in strained mercury telluride

To cite this article: O V Kibis *et al* 2019 *New J. Phys.* **21** 043016

New Journal of Physics
The open access journal at the forefront of physics

Deutsche Physikalische Gesellschaft DPG
IOP Institute of Physics

Published in partnership with: Deutsche Physikalische Gesellschaft and the Institute of Physics

OPEN ACCESS

RECEIVED
13 December 2018

REVISED
17 March 2019

ACCEPTED FOR PUBLICATION
27 March 2019

PUBLISHED
12 April 2019

PAPER

Structure of surface electronic states in strained mercury telluride

O V Kibis[1,2], O Kyriienko[3,4] and I A Shelykh[2,4]

[1] Department of Applied and Theoretical Physics, Novosibirsk State Technical University, Karl Marx Avenue 20, Novosibirsk 630073, Russia
[2] Science Institute, University of Iceland IS-107, Reykjavik, Iceland
[3] NORDITA, KTH Royal Institute of Technology and Stockholm University, Roslagstullsbacken 23, SE-106 91 Stockholm, Sweden
[4] ITMO University, Saint Petersburg 197101, Russia

E-mail: Oleg.Kibis@nstu.ru

Keywords: topological insulator, surface states, strained HgTe

Abstract

We present the theory describing the various surface electronic states arisen from the mixing of conduction and valence bands in a strained mercury telluride (HgTe) bulk material. We demonstrate that the strain-induced band gap in the Brillouin zone center of HgTe results in the surface states of two different kinds. Surface states of the first kind exist in the small region of electron wave vectors near the center of the Brillouin zone and have the Dirac linear electron dispersion characteristic for topological states. The surface states of the second kind exist only far from the center of the Brillouin zone and have the parabolic dispersion for large wave vectors. The structure of these surface electronic states is studied both analytically and numerically in the broad range of their parameters, aiming to develop its systematic understanding for the relevant model Hamiltonian. The results bring attention to the rich surface physics relevant for topological systems.

1. Introduction

The studies of two-dimensional (2D) electronic modes localized near the surface of a three-dimensional (3D) condensed matter structure (surface electronic states) represent one of the most actively studied directions of modern science of the last decade. The increasing interest of scientific community to this research area is caused by the topologically nontrivial nature of the surface states in structures of certain type known as topological insulators (TIs). Namely, TIs are condensed matter systems which behave like an insulator in their 3D bulk but have 2D gapless conducting electronic states protected by the time-reversal symmetry at their boundaries [1]. Up to date, such topologically protected electronic states were intensively studied theoretically and experimentally in various condensed matter structures [2–13], and their optical analogs were also revealed [14–18].

Particularly, it follows from the theoretical analysis based on the Z_2 topological invariants that the surface electronic states in bulk mercury telluride (HgTe) can be topologically nontrivial [3]. However, the band structure of natural HgTe is semi-metallic: there is the small overlap of conduction and valence bands originated from the bulk inversion asymmetry (BIA) of the crystal structure [19]. In order to observe the predicted topological surface states in HgTe, one needs to turn this semi-metal into insulator. To solve the problem, an uniaxial strain as a tool to open the band gap between the valence and conduction bands of HgTe was proposed [20]. Following this methodology, the topological surface states in strained HgTe were recently observed experimentally within the strain-induced band gap [21]. As a consequence, physical properties of the surface electronic states in strained HgTe-based materials are currently in the focus of attention [22–33]. However, the theory describing the structure of these surface states is still far from being complete. Particularly, the characteristic feature of HgTe is the coexistence of surface electronic states of different physical nature: besides of the discussed topological surface states in gapped HgTe, there are the surface states in gapless HgTe analyzed for the first time by D'yakonov and Khaetskii [34]. Certainly, the consistent theory should be able to describe the dependence of all surface states on the strain. The present article takes a step towards such a consistent theory and provides an intuitive understanding of the system.

The paper is organized as follows. In section 2, we formulate a formalism describing the surface electronic states of various kinds in strained HgTe. In section 3, we solve the corresponding Schrödinger problem analytically in the simplest particular cases, calculate the dispersion of the surface states numerically, and analyze their energy spectrum. The last two sections contain the conclusion and acknowledgments.

2. Model

We consider the surface electronic states which originate from the mixing of conduction and valence bands of HgTe near the center of the Brillouin zone (the electronic term Γ_8). In bulk strained HgTe, the states of this electronic term are described by the Hamiltonian [19]

$$\hat{\mathcal{H}} = \hat{\mathcal{H}}_{\rm L} + \hat{\mathcal{H}}_{\rm strain} + \hat{\mathcal{H}}_{\rm BIA}, \tag{1}$$

where

$$\hat{\mathcal{H}}_{\rm L} = \left(\gamma_1 + \frac{5}{2}\gamma_2\right)\mathbf{k}^2 - 2\gamma_2(J_x^2k_x^2 + J_y^2k_y^2 + J_z^2k_z^2) - 2\gamma_3(\{J_x, J_y\}k_xk_y + \{J_x, J_z\}k_xk_z + \{J_y, J_z\}k_yk_z) \tag{2}$$

is the conventional Luttinger Hamiltonian describing the conduction and valence bands of unstrained HgTe,

$$\hat{\mathcal{H}}_{\rm strain} = \left(a + \frac{5}{4}b\right)(u_{xx} + u_{yy} + u_{zz}) - b(J_x^2u_{xx} + J_y^2u_{yy} + J_z^2u_{zz}) - \frac{d}{\sqrt{3}}(\{J_x, J_y\}u_{xy} + \{J_x, J_z\}u_{xz} + \{J_y, J_z\}u_{yz}) \tag{3}$$

is the Bir-Pikus Hamiltonian describing the modification of conduction and valence bands of HgTe under strain, and

$$\hat{\mathcal{H}}_{\rm BIA} = \alpha[k_x\{J_x, (J_y^2 - J_z^2)\} + k_y\{J_y, (J_z^2 - J_x^2)\} + k_z\{J_z, (J_x^2 - J_y^2)\}] \tag{4}$$

is the term arisen from the BIA of HgTe crystal. Correspondingly, $\mathbf{k} = (k_x, k_y, k_z)$ is the electron wave vector, $\gamma_{1,2,3}$ are the Luttinger parameters of HgTe, a, b and d are the deformation potentials of HgTe, u_{ij} are the components of the deformation tensor of the strained HgTe, α is the BIA parameter, $J_{x,y,z}$ are the 4×4 matrices corresponding to the electron angular momentum $J = 3/2$, and the curly brackets $\{A, B\}$ represent anti-commutators of the matrices A and B. The eigenstates of the Hamiltonian (1) can be written in the most general form as four independent spinors,

$$\varphi_m = [C_{1m}, C_{2m}, C_{3m}\, C_{4m}]^T e^{i\mathbf{kr}}, \tag{5}$$

with indices $m = 1, 2, 3, 4$, and the spinor components $C_{nm}(k_x, k_y, k_z)$ are the functions of the electron wave vector, $\mathbf{k} = (k_x, k_y, k_z)$.

For definiteness, let us consider electronic states localized near the (001)-surface, assuming that the bulk HgTe fills the half-space for $z > 0$. It follows from the conservation laws that the surface (001) mixes different electronic states of the Hamiltonian (1) with the same energy, $\varepsilon(\mathbf{k}_s, k_z)$, and the same wave vector in the surface plane, $\mathbf{k}_s = (k_x, k_y)$, but with different normal components of the wave vector, k_z. As a consequence, the surface-localized electronic states which arise from the mixing are described by the same spinors (5) with the imaginary z-component of electron wave vector, $k_z = i\kappa$, where $\kappa > 0$ is the localization parameters, corresponding to the inverse of localization length for electronic states near the surface. Generally, the localization parameter, κ, can be a complex number but its real part must be positive. In bulk HgTe, there are the four different branches of electron energy, $\varepsilon(\mathbf{k})$, corresponding to the four branches of the conduction and valence bands spin-split due to the BIA terms of the Hamiltonian (1). Therefore, there are four different parameters, $\kappa_{1,2,3,4}(\mathbf{k}_s, \varepsilon)$, which can be found as four solutions of the secular equation,

$$\det|\hat{\mathcal{H}}(\mathbf{k}_s, i\kappa) - \varepsilon| = 0. \tag{6}$$

Making the replacement, $k_z \to i\kappa_{1,2,3,4}$, in the eigenspinors (5), we can write the surface-localized eigenfunction of the Hamiltonian (1) as a linear combination of the spinors,

$$\Psi = e^{i\mathbf{k}_s\mathbf{r}_s}\sum_{m=1}^{4}[C_{1m}(\mathbf{k}_s, i\kappa_m), C_{2m}(\mathbf{k}_s, i\kappa_m), C_{3n}(\mathbf{k}_s, i\kappa_m), C_{4n}(\mathbf{k}_s, i\kappa_m)]^T A_m e^{-\kappa_m z}, \tag{7}$$

where $\mathbf{r}_s = (x, y)$ is the electron radius-vector in the surface plane and $A_{1,2,3,4}$ are the constants to be determined. To do so, we chose the model of a surface potential which can be approximated by the infinitely-high barrier at position $z = 0$. This sets the boundary condition for the electron wave function (7) as $\Psi|_{z=0} = 0$, and results into the homogeneous system of four algebraic equations defining the constants A_j,

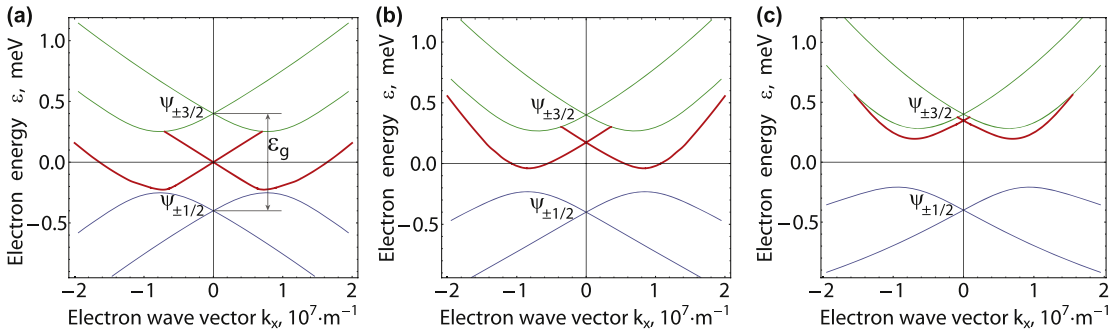

Figure 1. Structure of the surface electronic states (bold red curves) near the Brillouin zone center for the strain-induced gap $\varepsilon_g = 0.8$ meV and the different values of the Luttinger parameter γ_1: (a) $\gamma_1 = 0$; (b) $\gamma_1 = 7.8\ \hbar^2/2m_0$; (c) $\gamma_1 = 15.6\ \hbar^2/2m_0$ (the case of HgTe). Thin green and blue curves represent the dispersion of bulk conduction and valence bands which originate from the terms $\psi_{\pm 3/2}$ and $\psi_{\pm 1/2}$, respectively.

$$\sum_{m=1}^{4} A_m C_{nm}(\mathrm{k}_s, \mathrm{i}\kappa_m) = 0, \quad (n = 1, 2, 3, 4). \tag{8}$$

The secular equation of the algebraic system (8),

$$\det|C_{nm}(\mathbf{k}_s, \mathrm{i}\kappa_m)| = 0, \quad (n, m = 1, 2, 3, 4), \tag{9}$$

defines the sought energy spectrum of the surface electronic states, $\varepsilon(\mathbf{k}_s)$. In the next section of the article, we apply the strategy described above to find the spectrum $\varepsilon(\mathbf{k}_s)$ in systems with various band parameters. In the case of HgTe, we use the following parameters [28, 35]: $\gamma_1 = 15.6\hbar^2/2m_0$, $\gamma_2 = 9.6\ \hbar^2/2m_0$, $\gamma_3 = 8.6\ \hbar^2/2m_0$, $b = -1.22$ eV and $\alpha = 0.208$ Å·eV.

3. Results and discussion

In what follows, we consider the Hamiltonian (1) to be written as a 4×4 matrix in the conventional Luttinger–Kohn basis, ψ_{j_z}, corresponding to the different projections of electron angular momentum on the z axis, $j_z = \pm 1/2, \pm 3/2$ (see the appendix for details). In unstrained bulk HgTe, the four wave functions, ψ_{j_z}, are the eigenfunctions of the Hamiltonian (1): they describe the states of the electronic term Γ_8 at $\mathbf{k} = 0$, which are four-fold degenerate. As for strained bulk HgTe, we consider for definiteness the case of an uniaxial stress applied along the z axis. Under the uniaxial stress, the deformation tensor of HgTe, u_{ij}, written in the principal crystallographic axes, x, y, z, is diagonal. Particularly, the case of $u_{zz} < 0$ and $u_{xx} = u_{yy} > 0$ corresponds to the compressive strain, whereas the opposite case of $u_{zz} > 0$ and $u_{xx} = u_{yy} < 0$ corresponds to the tensile strain. As a result, the strain Hamiltonian (3) can be rewritten as

$$\hat{\mathcal{H}}_{\mathrm{strain}} = a(u_{xx} + u_{yy} + u_{zz}) + (\varepsilon_g/2)(J_z^2 - 5/4), \tag{10}$$

where $\varepsilon_g = 2b(u_{xx} - u_{zz}) = 2b(u_{yy} - u_{zz})$, and we note that $b < 0$ for HgTe. The first term of the Hamiltonian (10) is the strain-induced shift of zero energy, which will be omitted in the following. As for the second term, it describes the strain-induced splitting of the electronic states with $j_z = \pm 1/2$ and $j_z = \pm 3/2$ at $\mathbf{k} = 0$. It follows from the total Hamiltonian (1) with the strain Hamiltonian (10) that $\varepsilon_g = \varepsilon_{\pm 3/2} - \varepsilon_{\pm 1/2}$, where ε_{j_z} are the energies of these states at $\mathbf{k} = 0$ (see figure 1(a)). It should be noted, particularly, that the compressive strain ($\varepsilon_g < 0$) and the tensile strain ($\varepsilon_g > 0$) result in the opposite sequence orders for energies of the basic states with the wave functions $\psi_{\pm 1/2}$ and $\psi_{\pm 3/2}$. Substituting the strain Hamiltonian (3) into the total Hamiltonian (1), we can apply the methodology developed in section 2 to analyze the evolution of the surface electronic states in HgTe under stress.

First of all, let us consider the electronic states with the zero planar electron wave vector, $\mathbf{k}_s = 0$, which are localized near the (001)-surface of the uniaxially strained HgTe. The simplest case, which can be readily solved, corresponds to the Luttinger parameter $\gamma_1 = 0$. Physically, this model situation describes a semiconductor with the Hamiltonian (1), where the masses of electrons and holes along the z axis, m_e and m_h, are equal to each other, $m_e/m_h = (2\gamma_2 - \gamma_1)/(2\gamma_2 + \gamma_1)$. For such a symmetric electron–hole system, the Hamiltonian (1) at $\mathbf{k}_s = 0$ can be written in the Luttinger–Kohn basis as a block-diagonal matrix (see the appendix),

$$\hat{\mathcal{H}}_0 = \begin{bmatrix} -2\gamma_2\hat{k}_z^2 + \varepsilon_g/2 & \sqrt{3}\,\alpha\hat{k}_z & 0 & 0 \\ \sqrt{3}\,\alpha\hat{k}_z & 2\gamma_2\hat{k}_z^2 - \varepsilon_g/2 & 0 & 0 \\ 0 & 0 & 2\gamma_2\hat{k}_z^2 - \varepsilon_g/2 & -\sqrt{3}\,\alpha\hat{k}_z \\ 0 & 0 & -\sqrt{3}\,\alpha\hat{k}_z & -2\gamma_2\hat{k}_z^2 + \varepsilon_g/2 \end{bmatrix}, \tag{11}$$

where $\hat{k}_z = -i\partial/\partial z$ is the operator of the electron momentum normal to the considered surface. In the particular case of the Hamiltonian (11), the surface-localized eigenspinors (7) correspond to the eigenenergy $\varepsilon_0 = 0$ and can be written as

$$\begin{aligned} \Psi_1 &= D(\mathrm{e}^{-\kappa_+ z} - \mathrm{e}^{-\kappa_- z})[1,\ \mathrm{i},\ 0,\ 0]^T \\ \Psi_2 &= D(\mathrm{e}^{-\kappa_+ z} - \mathrm{e}^{-\kappa_- z})[0,\ 0,\ -\mathrm{i},\ 1]^T, \end{aligned} \tag{12}$$

where

$$\kappa_\pm = \frac{\sqrt{3}\,\alpha}{4\gamma_2} \pm \sqrt{\left(\frac{\sqrt{3}\,\alpha}{4\gamma_2}\right)^2 - \frac{\varepsilon_g}{4\gamma_2}} \tag{13}$$

are the localization parameters of the surface state, and $D = \sqrt{\sqrt{3}\,\alpha\varepsilon_g/(6\alpha^2 - 8\gamma_2\varepsilon_g)}$ is the normalization constant. The eigenspinors (12) can be easily verified by direct substitution into the Schrödinger equation, $\hat{\mathcal{H}}_0\Psi_{1,2} = \varepsilon_0\Psi_{1,2}$, with the Hamiltonian (11) and the eigenenergy $\varepsilon_0 = 0$. It follows from equation (13) that $\kappa_- < 0$ if $\varepsilon_g < 0$. Since the real part of both localization parameters, $\kappa_\pm$, must be positive, the surface states (12) exist only for $\varepsilon_g > 0$ (tensile strain). Physically, this means that the existence of the surface states (12), first, arises from the BIA terms ($\alpha \neq 0$) and, second, it strongly depends on the sequence order of their parent bulk states, $\psi_{\pm 1/2}$ and $\psi_{\pm 3/2}$.

To find the dispersion of the surface states (12) for small wave vectors $\mathbf{k}_s$, we have to project the total Hamiltonian (1) to the subspace spanned by these two states, $\{\Psi_1, \Psi_2\}$. Keeping the terms linear in $\mathbf{k}_s$, we arrive at the effective Hamiltonian,

$$\hat{\mathcal{H}}_{\mathrm{eff}} = \varepsilon_0 - \frac{3\alpha}{2}(\sigma_x k_x + \sigma_y k_y) - \frac{\sqrt{3}\,\alpha}{2}(\sigma_x k_y + \sigma_y k_x), \tag{14}$$

where $\sigma_{x,y}$ are the Pauli matrices written in the basis $\{\Psi_1, \Psi_2\}$. Diagonalizing the Hamiltonian (14), we can write the sought energy spectrum of the surface states (12) near $\mathbf{k}_s = 0$ as

$$\varepsilon(\mathbf{k}_s) = \varepsilon_0 \pm \sqrt{3}\,\alpha\sqrt{k_x^2 + k_y^2 + \sqrt{3}\,k_x k_y}. \tag{15}$$

It follows from equation (15) that the two degenerate states (12) form the Dirac point at $\mathbf{k}_s = 0$ with the energy $\varepsilon_0 = 0$ and anisotropic linear dispersion near the point. Applying the methodology of section 2, one can calculate numerically the dispersion of the surface states in the broad range of the wave vectors, $\mathbf{k}_s$. To demonstrate the properties of these surface states in more details, we plotted their dispersion for the HgTe band parameters $\gamma_{2,3}$ and α but for different Luttinger parameters γ_1 (see figure 1). In the model case of symmetric electron–hole system discussed above ($\gamma_1 = 0$), the Dirac point energy, $\varepsilon_0 = 0$, lies exactly in the middle of the bulk states $\psi_{\pm 1/2}$ and $\psi_{\pm 3/2}$ (see figure 1a), whereas the nonzero Luttinger parameter γ_1 shifts the Dirac point energy, ε_0, from the middle towards the bulk term $\psi_{\pm 3/2}$ (see figure 1(b)). As a result, the branches of the surface states are localized near the bulk term $\psi_{\pm 3/2}$ in the real case of HgTe (see figure 1(c)), where the electron–hole system is strongly asymmetric ($m_e/m_h \ll 1$). It should be stressed that the effective Hamiltonian (14) and the dispersion (15), which were derived formally for the particular case of $\gamma_1 = 0$, are applicable to describe the energy spectrum of surface states near the Dirac point for any band parameters and the strain-induced band gap. Namely, the energy of the Dirac point ε_0 is proportional to the band gap value, $\varepsilon_0 \propto \varepsilon_g$, where the proportionality constant depends on the bulk band parameters, $\gamma_{1,2,3}$ and α, and turns into zero if $\gamma_1 = 0$. Taking this into account, both the analytical expression for the Dirac dispersion (15) and the numerically calculated dispersion in figure 1(c) can be used to analyze the surface states in strained HgTe for any gap, $\varepsilon_g > 0$. Particularly, the Dirac velocity, $v_D = \sqrt{3}\,\alpha/\hbar$, which can be extracted from the dispersion (15), does not depend on the gap.

It follows from the aforesaid that the branches of the surface states merge into the spectrum of bulk electronic states if the plane electron wave vector, $\mathbf{k}_s$, is large enough (see figure 1(c)). Therefore, they exist only near $\mathbf{k}_s = 0$. However, there are the surface electronic states of other kind, which can exist far from $\mathbf{k}_s = 0$. In contrast to the states (12), the BIA Hamiltonian (4) is not crucial for their existence and will be omitted in the following analysis. To simplify calculations, we also will neglect the weak anisotropy of electron–hole dispersion in HgTe. Following [34], this neglect corresponds to the replacement of the Luttinger parameters, $\gamma_{2,3} \to \gamma = (2\gamma_2 + 3\gamma_3)/5$, in the Hamiltonian (2). Under these assumptions, the secular equation (9) reads

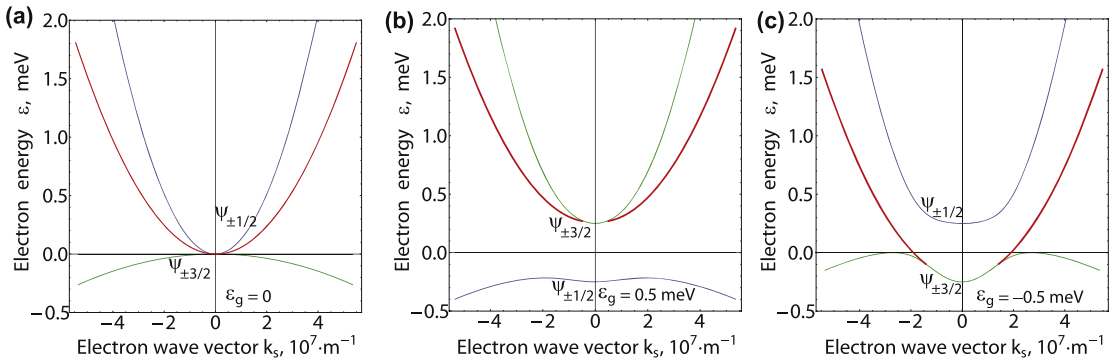

Figure 2. Structure of the D'yakonov–Khaetskii surface electronic states (bold red curves) in HgTe for the different strain-induced gaps ε_g:(a) unstrained material ($\varepsilon_g = 0$); (b) tensile strain ($\varepsilon_g = 0.5$ meV); (c) compressive strain ($\varepsilon_g = -0.5$ meV). Thin green and blue curves represent the dispersion of bulk bands which originate from the terms $\psi_{\pm 3/2}$ and $\psi_{\pm 1/2}$, respectively.

$$[\lambda_-^{(1)}\lambda_+^{(2)} - 1][\lambda_+^{(1)}\lambda_-^{(2)} - 1] = 0, \tag{16}$$

where

$$\lambda_\pm^{(j)} = \frac{\sqrt{3}\gamma(k_s^2 \mp 2k_s\kappa_j)}{\varepsilon - \gamma_1(k_s^2 - \kappa_j^2) + (-1)^j[\gamma(k_s^2 + 2\kappa_j^2) + \varepsilon_g/2]}, \tag{17}$$

$$\kappa_j = \sqrt{\frac{A + (-1)^j\sqrt{A^2 + 4BC}}{2B}}, \tag{18}$$

and

$$A = 2\gamma_1(\varepsilon - \gamma_1 k_s^2) + 2\gamma(4\gamma k_s^2 - \varepsilon_g),\ \ B = (\gamma_1 + 2\gamma)(2\gamma - \gamma_1),$$
$$C = (\varepsilon - \gamma_1 k_s^2)^2 - (\gamma k_s^2 + \varepsilon_g/2)^2 - 3\gamma^2 k_s^4.$$

Solving the equation (16) with equations (17) and (18), one can find the sought energy spectrum of the surface states, $\varepsilon(k_s)$, under the uniaxial strain. This spectrum is plotted in figure 2 for the different strain-induced gaps, ε_g. In the absence of the strain ($\varepsilon_g = 0$), equation (16) can be solved analytically and leads to the parabolic branch of the D'yakonov–Khaetskii (DKh) surface states [34],

$$\varepsilon(k_s) = \left[1 - \left(\frac{1 + \sqrt{3(2\gamma - \gamma_1)/(2\gamma + \gamma_1)}}{2}\right)^2\right](\gamma_1 + 2\gamma)k_s^2, \tag{19}$$

which is plotted in figure 2(a). Solving equation (16) numerically for $\varepsilon_g \neq 0$, we can plot the spectrum of the DKh surface states in strained HgTe. In contrast to the surface states discussed above, the DKh states exist for both tensile (see figure 2(b)) and compressive (see figure 2(c)) strain. However, their structure is crucially different for these two cases: in the case of tensile strain, the DKh states lie only within the bulk spectrum of conduction band (see figure 2(b)), whereas the case of compressive strain corresponds to the DKh states which lie also within the strain-induced band gap (see figure 2(c)). It should be noted also that the DKh states exist only for large electron wave vectors, k_s, and vanish near $k_s = 0$. It follows from figures 2(b) and (c) that the DKh branch merges into the continuum of bulk conduction band in the case of tensile strain (see figure 2(b)) and the continuum of bulk valence band in the case of compressive strain (see figure 2(c)) at a some critical electron wave vector. The value of the critical wave vector, $k_s = k_0$, is defined by equations (16)–(18), where the energy of the surface electron states, ε, is equal to the energy of one of the two bulk electron branches,

$$\varepsilon = \gamma_1 k_s^2 \pm \sqrt{(\gamma k_s^2 + \varepsilon_g/2)^2 + 3\gamma^2 k_s^4}. \tag{20}$$

Solving equations (16)–(18) together with equation (20), one can find that $k_0 \propto \sqrt{|\varepsilon_g|}$. Thus, the increase of the strain-induced gap ε_g shifts the existence domain of the DKh surface states to the region of large electron wave vectors, k_s. It follows from equation (16) that the spectrum of the DKh surface states in strained HgTe is parabolic and described approximately by equation (19) for large wave vectors, k_s, satisfying the condition $\gamma k_s^2 \gg \varepsilon_g$. It should be noted that the spectrum of the DKh surface states in strained materials of HgTe-class crucially depends on the Luttinger parameters. To demonstrate this, we plotted the dispersion of the DKh surface states in figure 3 for the HgTe band parameter $\gamma = 9.0\ \hbar^2/2m_0$ but for different Luttinger parameters γ_1. In the case of symmetric electron–hole system ($\gamma_1 = 0$) there are the two branches of the DKh states which behave as surface electrons and holes (see figure 3(a)). The nonzero Luttinger parameter γ_1 merges the upper (electronic) branch into the continuum of bulk electronic states and changes the curvature of the lower (hole) branch (see

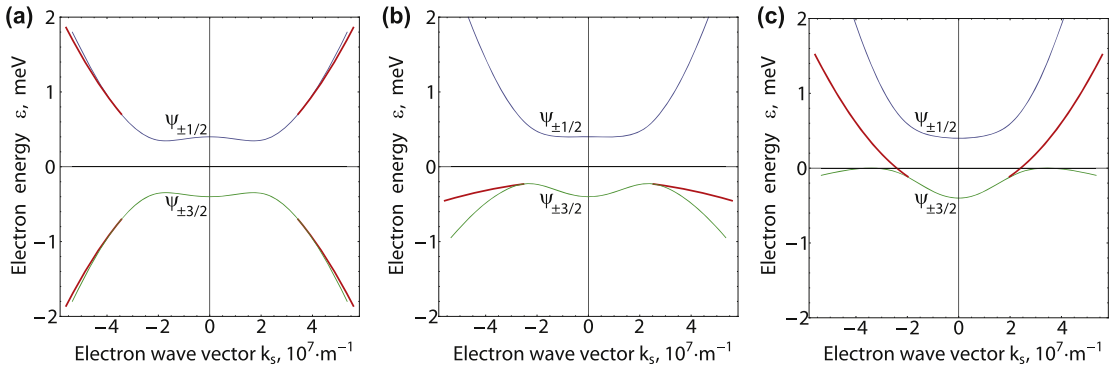

Figure 3. Structure of the D'yakonov–Khaetskii surface electronic states (bold red curves) for the strain-induced gap $\varepsilon_g = -0.8$ meV and the different values of the Luttinger parameter γ_1:(a) $\gamma_1 = 0$; (b) $\gamma_1 = 7.8\ \hbar^2/2m_0$; (c) $\gamma_1 = 15.6\ \hbar^2/2m_0$ (the case of HgTe). Thin green and blue curves represent the dispersion of bulk bands which originate from the terms $\psi_{\pm 3/2}$ and $\psi_{\pm 1/2}$, respectively.

figure 3(b)). As for the real case of HgTe parameters, only the lower branch survives and turns into the surface states of electronic kind (see figure 3(c)).

Finally, it should be noted that the experimental methodology based on the angle resolved photoemission spectroscopy (ARPES) technique, which is commonly used to study surface electronic states in various condensed matter structures [36], can allow to observe the surface states discussed above. It is important from an experimental viewpoint that the structure of all considered surface states crucially depends on the bulk Luttinger parameters, $\gamma_{1,2,3}$. Therefore, they should be chosen carefully to interpret experimental results adequately in HgTe-based materials (e.g. solid solutions CdHgTe and MnHgTe), where the band parameters depend on their stoichiometric composition.

4. Conclusion

We developed the theory describing the structure of various surface electronic states which appear due to the mixing of the conduction and valence bands in strained mercury telluride (HgTe). It predicts the coexistence of surface electronic states of two different kinds. First of them originate from the BIA of HgTe, have the linear Dirac dispersion, which is characteristic for topological states, and are localized in very narrow region of electron wave vectors near the Brillouin zone center. The surface states of second kind originate from the DKh surface states existing in gapless HgTe. Due to the strain-induced band gap, they are shifted far from the Brillouin zone center to the region of large electron wave vectors. Thus, the found surface states of the two kinds exist in different areas of the Brillouin zone and can be detected independently. The energy spectrum of the states and their structure are calculated both analytically and numerically in the broad range of band parameters.

Acknowledgments

The work was partially supported by Horizon2020 RISE project COEXAN, Russian Foundation for Basic Research (project 17-02-00053), Rannis project 163082-051, Ministry of Education and Science of Russian Federation (projects 3.457 3.2017/6.7, 3.261 4.2017/4.6, 14.Y26.31.0015), and the Government of the Russian Federation through the ITMO Fellowship and Professorship Program. OVK and OK thank the University of Iceland for hospitality.

Appendix. The Hamiltonian in the Luttinger–Kohn basis

The wave functions of the Luttinger–Kohn basis, ψ_{j_z}, corresponding to the different projections of electron angular momentum on the z axis, $j_z = \pm 1/2,\ \pm 3/2$, can be written as

$$\psi_{+3/2} = \frac{1}{\sqrt{2}}(X + \mathrm{i}Y)\uparrow, \psi_{-1/2} = -\frac{1}{\sqrt{6}}[(X - \mathrm{i}Y)\uparrow + 2Z\downarrow],$$
$$\psi_{+1/2} = \frac{1}{\sqrt{6}}[(X + \mathrm{i}Y)\downarrow - 2Z\uparrow], \psi_{-3/2} = -\frac{1}{\sqrt{2}}(X - \mathrm{i}Y)\downarrow, \quad \text{(A1)}$$

where the vertical arrows, $\uparrow$ and $\downarrow$, represent the spinors corresponding to the $\pm 1/2$ spin projections on the z axis, and X, Y, Z are the Bloch functions in the Brillouin zone center, which behave like the Cartesian coordinates,

x, y, z, under rotation of the coordinate axes [19]. In the basis (A1), the angular momentum matrices, $J_{x,y,z}$, read

$$J_x = \begin{bmatrix} 0 & 0 & \frac{\sqrt{3}}{2} & 0 \\ 0 & 0 & 1 & \frac{\sqrt{3}}{2} \\ \frac{\sqrt{3}}{2} & 1 & 0 & 0 \\ 0 & \frac{\sqrt{3}}{2} & 0 & 0 \end{bmatrix}, \; J_y = \begin{bmatrix} 0 & 0 & -i\frac{\sqrt{3}}{2} & 0 \\ 0 & 0 & i & -i\frac{\sqrt{3}}{2} \\ i\frac{\sqrt{3}}{2} & -i & 0 & 0 \\ 0 & i\frac{\sqrt{3}}{2} & 0 & 0 \end{bmatrix}, \; J_z = \begin{bmatrix} \frac{3}{2} & 0 & 0 & 0 \\ 0 & -\frac{1}{2} & 0 & 0 \\ 0 & 0 & \frac{1}{2} & 0 \\ 0 & 0 & 0 & -\frac{3}{2} \end{bmatrix}. \quad \text{(A2)}$$

Substituting the matrices (A2) into equation (1), we arrive at the Hamiltonian (1) written in the Luttinger–Kohn basis,

$$\hat{\mathcal{H}} = \begin{array}{c|cccc} \psi_{j_z} \backslash \psi_{j_z} & \psi_{+3/2} & \psi_{-1/2} & \psi_{+1/2} & \psi_{-3/2} \\ \psi_{+3/2} & F & I+L & H+M & N \\ \psi_{-1/2} & I^*+L & G & -N & -H+M \\ \psi_{+1/2} & H^*+M^* & -N^* & G & I-L \\ \psi_{-3/2} & N^* & -H^*+M^* & I^*-L & F \end{array}, \quad \text{(A3)}$$

where

$$F = (\gamma_1+\gamma_2)(k_x^2+k_y^2) + (\gamma_1-2\gamma_2)k_z^2 + (a-b)u_{zz} + (a+b/2)(u_{xx}+u_{yy}),$$
$$G = (\gamma_1-\gamma_2)(k_x^2+k_y^2) + (\gamma_1+2\gamma_2)k_z^2 + (a+b)u_{zz} + (a-b/2)(u_{xx}+u_{yy}),$$
$$I = -\sqrt{3}\gamma_2(k_x^2-k_y^2) + i2\sqrt{3}\gamma_3 k_x k_y - (\sqrt{3}b/2)(u_{xx}-u_{yy}) + id u_{xy}, \; M = -(\sqrt{3}\alpha/2)(k_x+ik_y),$$
$$H = -2\sqrt{3}\gamma_3(k_x-ik_y)k_z - d(u_{xz}-iu_{yz}), \; L = \sqrt{3}\alpha k_z, \; N = -(3\alpha/2)(k_x-ik_y).$$

In the particular case of the uniaxial strain along the z axis and $\gamma_1 = 0$, the matrix (A3) for $k_x = k_y = 0$ turns into the block-diagonal Hamiltonian (11).

ORCID iDs

O V Kibis https://orcid.org/0000-0003-3367-9980

References

[1] Hasan M Z and Kane C L 2010 Colloquium: Topological insulators *Rev. Mod. Phys.* **82** 3045
[2] Kane C L and Mele E J 2005 Z_2 topological order and the quantum spin hall effect *Phys. Rev. Lett.* **95** 146802
[3] Fu L and Kane C L 2007 Topological insulators with inversion symmetry *Phys. Rev.* B **76** 045302
[4] Fu L, Kane C L and Mele E J 2007 Topological insulators in three dimensions *Phys. Rev. Lett.* **98** 106803
[5] Moore J E and Balents L 2007 Topological invariants of time-reversal-invariant band structures *Phys. Rev.* B **75** 121306(R)
[6] Roy R 2009 Topological phases and the quantum spin Hall effect in three dimensions *Phys. Rev.* B **79** 195322
[7] Xia Y *et al* 2009 Observation of a large-gap topological-insulator class with a single Dirac cone on the surface *Nat. Phys.* **5** 398
[8] Zhang H, Liu C-X, Qi X-L, Dai X, Fang Z and Zhang S-C 2009 Topological insulators in Bi_2Se_3, Bi_2Te_3 and Sb_2Te_3 with a single Dirac cone on the surface *Nat. Phys.* **5** 438
[9] Chen Y L *et al* 2009 Experimental realization of a three-dimensional topological insulator, Bi_2Te_3 *Science* **325** 178
[10] Yudin D, Kibis O V and Shelykh I V 2016 Optically tunable spin transport on the surface of a topological insulator *New J. Phys.* **18** 103014
[11] Hasan M, Yudin D, Iorsh I V, Eriksson O and Shelykh I A 2017 Topological edge-state engineering with high-frequency electromagnetic radiation *Phys. Rev.* B **96** 205127
[12] Pervishko A A, Yudin D and Shelykh I A 2018 Impact of high-frequency pumping on anomalous finite-size effects in three-dimensional topological insulators *Phys. Rev.* B **97** 075420
[13] Kozin V K, Iorsh I V, Kibis O V and Shelykh I A 2018 Periodic array of quantum rings strongly coupled to circularly polarized light as a topological insulator *Phys. Rev.* B **97** 035416
[14] Lu L, Joannopoulos J D and Soljačić M 2014 Topological photonics *Nature Photon.* **8** 821
[15] Mittal S, Ganeshan S, Fan J, Vaezi A and Hafezi M 2016 Measurement of topological invariants in a 2D photonic system *Nature Photon.* **10** 180
[16] Whittaker C E *et al* 2018 Exciton polaritons in a two-dimensional Lieb lattice with spin–orbit coupling *Phys. Rev. Lett.* **120** 097401
[17] Klembt S *et al* 2018 Exciton-polariton topological insulator *Nature* **562** 552
[18] Banerjee R, Liew T C H and Kyriienko O 2018 Realization of Hofstadter's butterfly and a one-way edge mode in a polaritonic system *Phys. Rev.* B **98** 075412
[19] Bir G L and Pikus G E 1974 *Symmetry and Strain-Induced Effects in Semiconductors* (New York: Wiley)
[20] Dai X, Hughes T L, Qi X-L, Fang Z and Zhang S-C 2008 Helical edge and surface states in HgTe quantum wells and bulk insulators *Phys. Rev.* B **77** 125319
[21] Brüne C, Liu C X, Novik E G, Hankiewicz E M, Buhmann H, Chen Y L, Qi X L, Shen Z X, Zhang S C and Molenkamp L W 2011 Quantum hall effect from the topological surface states of strained bulk HgTe *Phys. Rev. Lett.* **106** 126803
[22] Maier L, Oostinga J B, Knott D, Brüne C, Virtanen P, Tkachov G, Hankiewicz E M, Gould C, Buhmann H and Molenkamp L W 2012 Induced superconductivity in the three-dimensional topological insulator HgTe *Phys. Rev. Lett.* **109** 186806

[23] Yan B and Zhang S-C 2012 Topological materials *Rep. Prog. Phys.* **75** 096501
[24] Oostinga J B, Maier L, Schüffelgen P, Knott D, Ames C, Brüne C, Tkachov G, Buhmann H and Molenkamp L W 2013 Josephson supercurrent through the topological surface states of strained bulk HgTe *Phys. Rev.* X **3** 021007
[25] Kozlov D A, Kvon Z D, Olshanetsky E B, Mikhailov N N, Dvoretsky S A and Weiss D 2014 Transport properties of a 3D topological insulator based on a strained high-mobility HgTe film *Phys. Rev. Lett.* **112** 196801
[26] Dantscher K-M *et al* 2015 Cyclotron-resonance-assisted photocurrents in surface states of a three-dimensional topological insulator based on a strained high-mobility HgTe film *Phys. Rev.* B **92** 165314
[27] Li J, He C, Meng L, Xiao H, Tang C, Wei X, Kim J, Kioussis N, Stocks G M and Zhong J 2015 Two-dimensional topological insulators with tunable band gaps: single-layer HgTe and HgSe *Sci. Rep.* **5** 14115
[28] Ruan J, Jian S-K, Yao H, Zhang H, Zhang S-C and Xing D 2016 Symmetry-protected ideal Weyl semimetal in HgTe-class materials *Nat. Commun.* **7** 11136
[29] Kirtschig F, van den Brink J and Ortix C 2016 Surface-state spin textures in strained bulk HgTe: strain-induced topological phase transitions *Phys. Rev.* B **94** 235437
[30] Leubner P, Lunczer L, Brüne C, Buhmann H and Molenkamp L W 2016 Strain engineering of the band gap of HgTe quantum wells using superlattice virtual substrates *Phys. Rev. Lett.* **117** 086403
[31] Haas B, Thomas C, Jouneau P-H, Bernier N, Meunier T, Ballet P and Rouvière J-L 2017 High precision strain mapping of topological insulator HgTe/CdTe *Appl. Phys. Lett.* **110** 263102
[32] Grendysa J, Tomaka G, Sliz P, Becker C R, Trzyna M, Wojnarowska-Nowak R, Bobko E and Sheregii E M 2017 MBE growth of topological isolators based on strained semi-metallic HgCdTe layers *J. Cryst. Growth.* **480** 1
[33] Thomas C, Crauste O, Haas B, Jouneau P-H, Bäuerle C, Lévy L P, Orignac E, Carpentier D, Ballet P and Meunier T 2017 Revealing topological Dirac fermions at the surface of strained HgTe thin films via quantum Hall transport spectroscopy *Phys. Rev.* B **96** 245420
[34] D'yakonov M I and Khaetskii A V 1981 Surface states in a gapless semiconductor *JETP Lett.* **33** 110
[35] Adachi S 2004 *Handbook of Physical Properties of Semiconductors: Vol.3, II-VI Compound Semiconductors* (New York: Kluwer)
[36] Chen Y 2012 Studies on the electronic structures of three-dimensional topological insulators by angle resolved photoemission spectroscopy *Front. Phys.* **7** 175